IceModel Technical Document

Matthew G. Cooper[1*]

[1]Atmospheric, Climate, and Earth Sciences Division, Pacific Northwest National Laboratory, 902 Battelle Blvd, Richland, 99354, WA, USA.

Corresponding author(s). E-mail(s): matt.cooper@pnnl.gov;

Contents

List of Figures

1 IceModel technical description

1.1 Heat equation

IceModel solves the unsteady one-dimensional heat equation:

$$\frac{\partial H}{\partial t} = \frac{\partial F}{\partial z} + S \tag{1}$$

where H [J m^{-3}] is enthalpy per unit volume, t [s] is time, F [W m^{-2}] is net heat flux along vertical dimension z [m], and S [W m^{-3}] is a heat source/sink term. The enthalpy of the mixture of ice, liquid water and water vapor is defined following Jordan (1991):

$$H = \int_{T_{\text{ref}}}^{T} \left(\rho_i \theta_i c_i + \rho_\ell \theta_\ell c_\ell + L_f \rho_\ell \frac{\partial \theta_\ell}{\partial T} + L_v \theta_v \frac{\partial \rho_v}{\partial T} \right) dT. \tag{2}$$

Here, T [K] is temperature, $T_{\text{ref}} = 273.16$ K is the triple-point temperature of water, ρ_i [kg m^{-3}] is ice density, ρ_ℓ [kg m^{-3}] is liquid water density, θ_i [m^3 m^{-3}] is volumetric ice fraction, θ_ℓ [m^3 m^{-3}] is volumetric liquid water fraction, c_i [J kg^{-1} K^{-1}] is specific heat capacity of ice, c_ℓ [J kg^{-1} K^{-1}] is specific heat capacity of liquid water, L_f [J kg^{-1}] is latent heat of fusion of ice, $\rho_{v,\text{sat}}$ [kg m^{-3}] is saturation water vapor density, L_v [J kg^{-1}] is latent heat of vaporization of ice, and θ_v [m^3 m^{-3}] is volumetric water vapor fraction. Equation 2 neglects sensible heat effects associated with water vapor and dry air, and assumes that the system is isolated from work interactions with its surroundings.

Fluxes across internal layers ($z > z_{\text{sfc}}$) are driven by heat conduction and vapor diffusion through the ice matrix:

$$F(z > z_{\text{sfc}}) = -k_e \frac{\partial T}{\partial z} \tag{3}$$

where the mixture effective thermal conductivity, k_e [W m^{-1} K^{-1}], is:

$$k_e = \theta_i k_i + \theta_\ell k_\ell + \theta_v k_v. \tag{4}$$

Here, k_ℓ [W m^{-1} K^{-1}] is the thermal conductivity of liquid water, the thermal conductivity of the ice, k_i, is modeled by Equation 5 of Calonne et al (2019), and the thermal diffusivity of the vapor, k_v [W m^{-1} K^{-1}], is

$$k_v = D_e L_v \frac{\partial \rho_{v,\text{sat}}}{\partial T} \tag{5}$$

where,

$$\frac{\partial \rho_{v,\text{sat}}}{\partial T} = \frac{1}{R_v T}\left(\frac{\partial P_{v,\text{sat}}}{\partial T} - \frac{P_{v,\text{sat}}}{T}\right). \tag{6}$$

The vapor diffusivity, D_e [m^2 s^{-1}], is given by Anderson (1976):

$$D_e = 9.0 \times 10^{-5}\left(\frac{T}{T_\text{ref}}\right)^{n_D}, \tag{7}$$

and the saturation vapor pressure, $P_{v,\text{sat}}$ [Pa], is defined following Buck (1981):

$$P_{v,\text{sat}} = P_{v0,\text{sat}} \exp\left[\frac{b(T - T_\text{ref})}{c + T - T_\text{ref}}\right]. \tag{8}$$

The liquid water fraction, θ_ℓ, is related to the depression temperature, $T_D = T_\text{ref} - T$, by the phase fraction characteristic function (Jordan, 1991; Clark et al, 2021):

$$\frac{\theta_\ell}{\theta_w} = \frac{1}{1 + [a(T_\text{ref} - T)]^2}, \tag{9}$$

and,

$$\frac{\partial \theta_l}{\partial T} = 2a^2(T_\text{ref} - T)(\theta_\ell^2/\theta_w) \tag{10}$$

where,

$$\theta_w = \theta_\ell + \theta_i(\rho_i/\rho_\ell) \tag{11}$$

is the volumetric total water fraction.

The heat flux at the surface, $F(z = z_{\text{sfc}})$ [W m^{-2}], couples the subsurface ice column to the atmosphere:

$$F(z = z_{\text{sfc}}) = Q_{\downarrow}^{SW}(1-\alpha)\chi + \varepsilon(Q_{\downarrow}^{LW} - \sigma T_{\text{sfc}}^4) + Q_H + Q_E + Q_c \tag{12}$$

where,

$$Q_c = k_e \frac{\partial T}{\partial z}\bigg|_{z=z_{\text{sfc}}} \tag{13}$$

is the conductive heat flux, $Q_{\downarrow}^{SW}$ is the downward shortwave (solar) radiation flux, α [-] is the surface albedo, χ [-] is the fraction of the net solar radiation flux absorbed in the surface layer, ε [-] is the surface emissivity, $Q_{\downarrow}^{LW}$ is the downward longwave radiation flux, σ [W m^{-2} K^{-4}] is the Stefan-Boltzmann constant, and T_{sfc} [K] is the surface temperature. The sensible heat flux Q_H, and the latent heat flux Q_E, are calculated using Monin-Obukhov similarity theory following methods described in Liston et al (1999).

1.2 Two-stream radiative transfer model

Subsurface absorption of transmitted solar radiation is represented by the source term:

$$S(z > z_{\text{sfc}}) = \frac{\partial Q_s}{\partial z} \tag{14}$$

where the subsurface net radiative flux, Q_s [W m^{-2}], is modeled with the two-stream radiative transfer method described by Schlatter (1972), updated with spectral detail

following Brandt and Warren (1993):

$$Q_s(z) = Q^{\uparrow} - Q^{\downarrow} \tag{15}$$

$$\mathrm{d}Q^{\uparrow} = (aQ^{\uparrow} + rQ^{\uparrow} - rQ^{\downarrow})\mathrm{d}z \tag{16}$$

$$\mathrm{d}Q^{\downarrow} = (-aQ^{\downarrow} - rQ^{\downarrow} + rQ^{\uparrow})\mathrm{d}z \tag{17}$$

$$a = \eta(z)\left(\frac{1-\alpha}{1+\alpha}\right), \quad r = \eta(z)\left(\frac{2\alpha}{1-\alpha^2}\right), \tag{18}$$

where $Q^{\uparrow}$ and $Q^{\downarrow}$ are the upward and downward fluxes at level z, respectively, and a and r are the absorptivity and reflectivity of level z, respectively. The spectrally integrated downward flux extinction coefficient, $\eta(z)$ [m^{-1}], is given by Brandt and Warren (1993):

$$\eta(z) = -\frac{1}{\Delta z}\ln\left[\frac{\int Q_{\lambda}^{\downarrow}\exp[-k_{\lambda}(z+\Delta z)]\mathrm{d}\lambda}{\int Q_{\lambda}^{\downarrow}\exp[-k_{\lambda}(z)]\mathrm{d}\lambda}\right] \tag{19}$$

where $Q_{\lambda}^{\downarrow}$ [W m^{-2} nm^{-1}] is the downward spectral shortwave radiation flux at the ice surface for wavelength λ, k_{λ} [m^{-1}] is the spectral flux extinction coefficient for wavelength λ:

$$k(\lambda) = \sigma_{\mathrm{ext}}(\lambda)\sqrt{(1-\omega(\lambda))(1-g(\lambda)\omega(\lambda))}, \tag{20}$$

and,

$$\sigma_{\mathrm{ext}}(\lambda) = \frac{3}{4}\frac{Q_{\mathrm{ext}}(\lambda)}{r_{\mathrm{eff}}} \tag{21}$$

is the single-scattering extinction coefficient. Values for the single-scattering extinction efficiency $Q_{\mathrm{ext}}(\lambda)$, the co-albedo $1-\omega(\lambda)$, and the scattering anisotropy $g(\lambda)$ were calculated as functions of grain size, r_{eff}, using Mie scattering algorithms provided as MATLAB code by Mätzler (2002) and the complex index of refraction of pure ice from Warren and Brandt (2008). The Mie solutions at each wavelength were integrated over a Gaussian size distribution ($N = 1000$) of scattering radii $\mathcal{N}(\mu = 2.0\,\mathrm{mm}, \sigma =$

0.3 mm) to eliminate ripples associated with the Bessel function solutions to the Mie equations (Fig. 1) (Bohren and Huffman, 2007).

Equation 20 represents the spectral flux extinction in a scattering and absorbing medium composed of ice and liquid water. Absorption of visible light by impurities contained within the ice matrix is represented by Equation 15 of Warren et al (2006):

$$k(\lambda) = k(\lambda_0)\sqrt{\frac{k_{\text{abs}}(\lambda)}{k_{\text{abs}}(\lambda_0)}}, \quad 300 < \lambda < 700\,\text{nm} \tag{22}$$

where $\lambda_0 = 600\,\text{nm}$ is a reference wavelength. Values for $k_{\text{abs}}(\lambda)$ used as input to Equation 22 were obtained from measurements of spectral flux extinction within glacier ice in Greenland's western ablation zone (Fig. 2) (Cooper et al, 2021).

1.3 Numerical implementation

Following Patankar (1980), we develop a conservative finite volume discretization of the heat equation, by integrating Equation 1 over a control volume of thickness Δz, and a time interval from t to $t + \Delta t$:

$$\int_z^{z+\Delta z}\int_t^{t+\Delta t}\frac{\partial H}{\partial t}\,dt\,dz = \int_t^{t+\Delta t}\int_z^{z+\Delta z}\frac{\partial F}{\partial z}\,dz\,dt + S, \tag{23}$$

which yields the following discretized equation under a fully-implicit time integration:

$$\Delta H \Delta z = \left(k_e \frac{\mathrm{d}T}{\mathrm{d}z}\right)\Delta t + \Delta Q_s \Delta t. \tag{24}$$

The change in enthalpy, ΔH [J m^{-3}], is represented by a Taylor expansion (Swaminathan and Voller, 1993; Clark et al, 2021):

$$\Delta H^{i+1} = \Delta H^i + \left(\frac{\mathrm{d}H}{\mathrm{d}T}\right)^i \Delta T^{i+1} \tag{25}$$

where i indexes nonlinear iterations within a timestep, $\Delta T^{i+1} = T^{i+1} - T^i$ is the temperature change over one iteration, and $\Delta H^i = H^i - H^o$, where o indexes "old" values at the start of a timestep, prior to the first iteration.

Substituting the expanded enthalpy expression into Equation 24, we obtain the following conservative discretization of the heat equation:

$$\Delta H^i + \left(\frac{\mathrm{d}H}{\mathrm{d}T}\right)^i \Delta T^{i+1} = \frac{\Delta t}{\Delta z}\left(k_e \frac{\mathrm{d}T}{\mathrm{d}z} + \Delta Q_s\right)^i \tag{26}$$

where $\mathrm{d}H/\mathrm{d}T$ is given by the integrand of Equation 2.

Equation 26 is equivalent to the optimal enthalpy scheme defined by Equations 17–18 and Equation 24 of Swaminathan and Voller (1993). Operationally, Equation 26 is cast in a tridiagonal form and solved for the current temperature field, T^{i+1}, which is then corrected to be consistent with the current enthalpy field, H^{i+1}, updated with Equation 25 (Swaminathan and Voller, 1993).

Following each successful iteration, if the ice fraction θ_i of the upper layer drops below a prescribed 10% threshold, it merges with the layer directly beneath it. Like Equation 26, this combination process is governed by the principle of enthalpy conservation. Following Equation 139 of Jordan (1991), the sum of the enthalpies of the individual layers is equated to the enthalpy of the combined layer. This calculation results in a third-order polynomial equation in terms of the temperature of the combined layer. The root of the polynomial is efficiently located using a derivative-free optimization based on Brent's method.

The system of equations is solved on a uniform mesh with a 4 cm node spacing extending from a surface datum ($z = z_{\mathrm{sfc}}$) to a depth of 20 m. The spectral model provides the source term ΔQ_s on a uniform mesh with a 2 mm node spacing extending from the surface to a depth of 12 m, following the method of solution detailed in Appendix 1 of Schlatter (1972). At the upper boundary, Equation 12 is solved for the

ice surface temperature T_{sfc} using Newton-Rhapson iteration. At the lower boundary, a zero-flux condition is assumed:

$$k_e \frac{\partial T}{\partial z}\bigg|_{z=z_{\max}} = 0 \tag{27}$$

where an initial value $T(z_{\max}) = -8.0$ ∘C is prescribed from measurements of ice temperature in Greenland's western ablation zone (Hills et al, 2018).

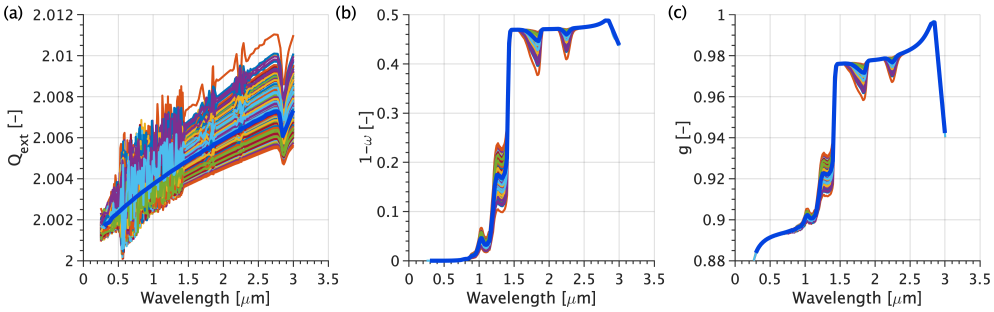

Fig. 1 Scattering coefficients for two-stream radiative transfer model. (a) Single-scattering extinction coefficient Q_{ext}, (b) single-scattering co-albedo $1-\omega$, and (c) asymmetry parameter g, computed using Mie scattering algorithms for a grain size ensemble ($N = 1000$) following a normal distribution with a mean of 2.0 mm and a standard deviation of 0.3 mm. Ensemble averages for 118 spectral bands covering the solar spectrum (0.3–3.03 μm) are displayed as thick blue lines.

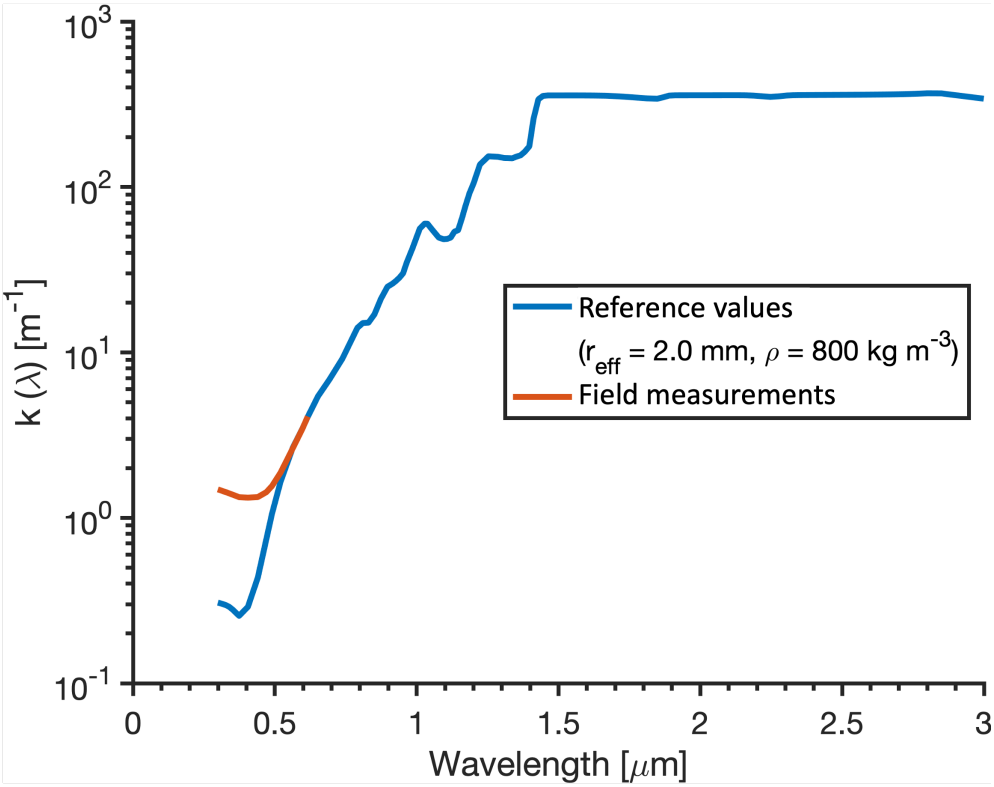

Fig. 2 Spectral flux extinction coefficients for glacier ice. Values of the flux extinction coefficient $k(\lambda)$ from 0.3–3.0 μm, for an ice volume with an effective optical grain radius of $r_{\text{eff}} = 2.0 \pm 0.3$ mm and a bulk density of $\rho = 800\,\text{kg/m}^3$. Reference values for these coefficients are calculated using Equation 20 and the single scattering coefficients presented in Fig. 1 for an optically pure glacier ice volume. The observed values are from Equation 22 using ice absorption coefficient values derived from measurements in the study area (Cooper et al, 2021), with elevated values in the spectral region 0.3–0.7 μm attributed to the presence of light-absorbing impurities within the ice.

References

Anderson EA (1976) A point energy and mass balance model of a snow cover. Technical Report 19, Office of Hydrology, National Weather Service

Bohren CF, Huffman DR (2007) Absorption and Scattering of Light by Small Particles. John Wiley & Sons, Ltd

Brandt RE, Warren SG (1993) Solar-heating rates and temperature profiles in Antarctic snow and ice. Journal of Glaciology 39(131):99–110. https://doi.org/10.3189/S0022143000015756

Buck AL (1981) New Equations for Computing Vapor Pressure and Enhancement Factor. Journal of Applied Meteorology 20(12):1527–1532. https://doi.org/10.1175/1520-0450(1981)020<1527:NEFCVP>2.0.CO;2

Calonne N, Milliancourt L, Burr A, et al (2019) Thermal Conductivity of Snow, Firn, and Porous Ice From 3-D Image-Based Computations. Geophysical Research Letters 46(22):13079–13089. https://doi.org/10.1029/2019GL085228

Clark MP, Zolfaghari R, Green KR, et al (2021) The Numerical Implementation of Land Models: Problem Formulation and Laugh Tests. Journal of Hydrometeorology 22(6):1627–1648. https://doi.org/10.1175/JHM-D-20-0175.1

Cooper MG, Smith LC, Rennermalm ÅK, et al (2021) Spectral attenuation coefficients from measurements of light transmission in bare ice on the Greenland Ice Sheet. The Cryosphere 15(4):1931–1953. https://doi.org/10.5194/tc-15-1931-2021

Hills BH, Harper JT, Meierbachtol TW, et al (2018) Processes influencing heat transfer in the near-surface ice of Greenland's ablation zone. The Cryosphere 12(10):3215–3227. https://doi.org/10.5194/tc-12-3215-2018

Jordan R (1991) A One-Dimensional Temperature Model For a Snowpack. Special Report 91-16, Cold Regions Research and Engineering Laboratory, Hanover, NH

Liston GE, Bruland O, Elvehøy H, et al (1999) Below-surface ice melt on the coastal Antarctic ice sheet. Journal of Glaciology 45(150):273–285. https://doi.org/10.3189/002214399793377130

Mätzler C (2002) MATLAB Functions for Mie Scattering and Absorption, Version 2. Research Report 2002-11, Institut für Angewandte Physik, Bern, Switzerland. https://boris.unibe.ch/146550/, https://doi.org/10.7892/BORIS.146550

Patankar SV (1980) Numerical Heat Transfer and Fluid Flow. Series in Computational Methods in Mechanics and Thermal Sciences, Hemisphere Publishing Corporation

Schlatter TW (1972) The Local Surface Energy Balance and Subsurface Temperature Regime in Antarctica. Journal of Applied Meteorology 11(7):1048–1062. https://doi.org/10.1175/1520-0450(1972)011<1048:TLSEBA>2.0.CO;2

Swaminathan C, Voller V (1993) ON THE ENTHALPY METHOD. International Journal of Numerical Methods for Heat & Fluid Flow 3(3):233–244. https://doi.org/10.1108/eb017528

Warren SG, Brandt RE (2008) Optical constants of ice from the ultraviolet to the microwave: A revised compilation. Journal of Geophysical Research: Atmospheres 113(D14):D14220. https://doi.org/10.1029/2007JD009744

Warren SG, Brandt RE, Grenfell TC (2006) Visible and near-ultraviolet absorption spectrum of ice from transmission of solar radiation into snow. Applied Optics 45(21):5320–5334. https://doi.org/10.1364/AO.45.005320